UNIVERSITÀ DEGLI STUDI DI BARI

DIPARTIMENTO INTERATENEO DI FISICA

"Michelangelo Merlin"

Livio Nicola Carenza

II Year Report

In this brief essay I will report on the research activity that I carried on during the second year of my PhD.

My research is basically focused on Soft Matter topics, concerning both Liquid Crystals and Active Matter, from a theoretical standpoint. In the last decades, research in these fields has shed light on the physical properties of such systems that are often implemented in the the design of novel materials and technological devices. Nevertheless, they are also an important benchmark for the understanding of some theoretical problems that still remain unsolved, such as the onset of mesoscopic turbulence or the development of topological defects in condensed matter.

The theoretical description of (living) liquid crystals requires the treatment of the flow $\boldsymbol{v}$ of the underlying fluid and a field theory to capture the physical properties and the dynamics of the suspended units. Hydrodynamics is ruled by a generalized Navier-Stokes equation

$$\rho \left(\partial_t + \boldsymbol{v} \cdot \nabla \right) \boldsymbol{v} = \nabla \cdot \underline{\underline{\sigma}}, \tag{1}$$

where the stress tensor $\underline{\underline{\sigma}}$ contains non-newtonian contributions, capturing the forces exerted by the long molecules or the active agents, whose state is in turn described by a suitable order parameter ($\boldsymbol{P}$ in the following), evolving in accordance to a advective-relaxing equation:

$$\frac{d\boldsymbol{P}}{dt} = -\frac{\boldsymbol{h}}{\Gamma}. \tag{2}$$

The coupling of these two equation gives rise to the *nemato-hydrodynamics* and constitutes a fascinating field, only partially explored.

In what follows I will first go through a brief introduction concerning the state of the art of theoretical research in Active Fluids and open problems in this scope and I will present a field theory approach for the modelling of (active) liquid crystals and the basic features of the lattice Boltzmann method, the numerical scheme that I implemented to integrate the nemato-hydrodynamic equations. In the following Sections I will present some advancements that I obtained in my research scope, briefly listed in the following:

- The development of a novel model to describe confined active gels in bidimensional geometries allowed to reproduce the dynamical behavior of suspension of bacteria and cytoskeletal extracts.
- The Fourier characterization of multi-scale flow interaction typical of the chaotic state occurring in active gels was compared with the Kolmogorov theory for fully developed turbulence in Newtonian fluids.
- The rheological analysis of *negative-viscosisity states* occurring in active systems when excited by an external forcing, was able to shed light on the occurrence of a superfluidic regime in bacterial systems.

1 Theoretical Aspects in Active Matter

Active fluids are living matter or biologically inspired systems with the common characteristic of being composed by self-propelled (or active) units that burn stored energy and turn it into work, giving rise, eventually, to systematic and collective movements. These systems evolve inherently far from thermodynamic equilibrium due to the internal energy that the active constituents continuously inject in the system at a characteristic lengthscale much smaller than the system size.

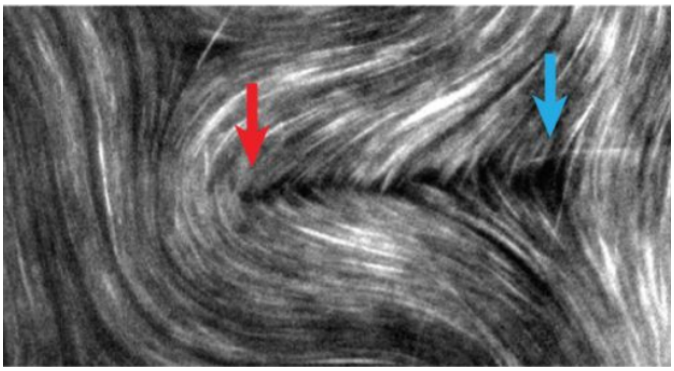

Figure 1: Active microtubule bundles arrange in a nematic fashion. Activity produces flows that advect the constituents eventually leading to the generation of topological defects (see arrows).

Living matter offers a wide variety of realizations of active systems, ranging from macroscopic lengthscales (flock of birds, schools of fish, insects swarms) to microscopical ones (bacterial suspensions, cytoskeleton extracts, eukaryotic cells in a tissue or on a substrate). While the nature of these systems might considerably differ, they still exhibit a certain number of common properties such as orientational order. Active constituents are in general anisotropic, and this defines a preferential orientation for their self-propulsion or the force they apply on their surroundings. Because of their anisotropy, active consitutents often prefer to align next to each other, thus giving rise to patterns that strongly resemble those found in passive Liquid Crystals.

At the same time, active systems are characterized by non-equilibrium properties that do not always find an equivalent in their passive counterpart. One of the key differences is the injection of energy at small scales (i.e. the size of the active agents). This leads to developing hydrodynamic instabilities with a number of fascinating phenomena.

On the experimental side, the complex features of active matter have been widely studied to understand their topological properties, as in the experiment by Sanchez et al.[1], where microtubule filaments were made 'active' by the addition of kinesin, molecular motors capable of converting chemical energy from ATP hydrolysis into mechanical motion of the filaments themselves; at high concentration of the active agents, hydrodynamic instabilities were found to sustain autonomous flows, eventually breaking the long-range orientational order by generating pairs of oppositely charged topological defects (see for instance Fig. 1).

If the strength of active forcing is very intense compared with the elastic properties of the active gel, the dynamics of the system becomes chaotic, a behavior addressed as *active turbulence*. This is highly surprising since biological systems usually evolve at very low Reynolds numbers, due to the reduced length-scale of the flows. Under this conditions, dissipation phenomena overcome advective mechanisms, that are in turn responsible for the onset of classic turbulence in a Newtonian (passive) fluid.

Another fascinating topic in active matter concerns the rheological properties of active fluids. Recently, some experiments have shown the occurence of negative viscosity states in bacterial suspensions. Bacteria are indeed capable of swimming in an ordered fashion, thus exciting flows whose intensity may be orders of magnitude greater than the speed accessible by a single unit. When subject to an external shear, bacteria may organize to counterbalance the imposed flow, by applying a net force on the walls thus leading to a situation where the overall behavior of the

[1]Tim Sanchez, Daniel T. N. Chen, Stephen J. DeCamp, Michael Heymann, and Zvonimir Dogic. Spontaneous motion in hierarchically assembled active matter. Nature, 491:431,434, 2012.

suspension is similar to a superfluid, eventually inverting the flow, with consequent development of an effective negative viscosity.

2 A continuum model for active emulsions

Many theoretical models have been developed to reproduce the behavior of active sytems in fluid environments, ranging from a molecular dynamic approach (where the dynamics of the single constituents is taken into account) to minimal hydrodynamic approach (as the Slomka-Dunkel model, where super-viscous terms are included to provide energy-injection at small length-scales). In my research I make use of the active-gel model. This is a meso-scale approach where the single constituents are traced out by a coarse-grain over the small length-scales and relevant information is encoded in a few dynamical fields evolving in accordance to suitable evolution equations.

In order to describe a suspension of active constituents a concentration (scalar) field ϕ is used, while their mean (local) orientation is given by the polarization (vector) field $\boldsymbol{P}$. The velocity field $\boldsymbol{v}$ is assumed to be divergence-free, since in experiments on active fluids comprimibility effects are highly suppressed (*i.e.* the density ρ is uniform and constant) as the velocity are very low ($\sim 10\mu m/s$).

By assuming that the amount of active constituents is conserved, one can require the dynamics of the concentration ϕ to be ruled by a convection diffusion equation:

$$\frac{\partial \phi}{\partial t} + \nabla \cdot (\phi \mathbf{v}) = M \nabla^2 \mu, , \tag{3}$$

where M is the mobility and $\mu = \delta \mathcal{F}/\delta\phi$ is the chemical potential (being $\mathcal{F}$ a suitable free energy functional which defines the equilibrium properties of the system). The polarization field follows a Beris-Edwards evolution:

$$\frac{\partial \boldsymbol{P}}{\partial t} + (\mathbf{v} \cdot \nabla)\, \boldsymbol{P} = -\underline{\underline{\Omega}} \cdot \boldsymbol{P} + \xi \underline{\underline{D}} \cdot \boldsymbol{P} - \frac{\boldsymbol{h}}{\Gamma}. \tag{4}$$

Here $\underline{\underline{D}}$ and $\underline{\underline{\Omega}}$ are respectively the symmetric and antisymmetric parts of the strain tensor $\nabla \boldsymbol{v}$, ξ is the alignment parameter, ruling the response of the polar field to a shear flow, Γ is the rotational viscosity and $\boldsymbol{h} = \delta \mathcal{F}/\delta \boldsymbol{P}$ is the molecular field that drives the fields towards the equilibrium configuration. The hydrodynamics is governed by the Navier-Stokes equation:

$$\rho\, (\partial_t + \boldsymbol{v} \cdot \nabla)\, \boldsymbol{v} = -\nabla P + \nabla \cdot (\underline{\underline{\sigma}}^{pass} + \underline{\underline{\sigma}}^{act}). \tag{5}$$

Here the pressure term P enforces the incompressibility condition, while the stress tensor has been divided in two contributions: a passive term $\underline{\underline{\sigma}}^{pass}$ including reactive and dissipative contributions (such as elastic stress and viscosity) and an active term $\underline{\underline{\sigma}}^{act}$. This is a phenomenological contribution derived from a coarse graining procedure. In general, the propulsive motion of active agents dispersed in a fluid creates a circulating flow pattern around each swimmer. The specific swimming mechanism of bacteria, for example, causes fluid to be expelled both forwards and backwards along the fore-aft axis, and drawn inwards radially towards this axis, creating an extensile flow pattern. In some cytoskeleton extracts (such as the actomyosin protein complex), motor proteins can pull the filaments amongst themselves, causing them to contract lengthwise and giving rise to a contractile flow opposite to that described for extensile stresses (Fig. 2). By summing the contributions from each force dipole and coarse-graining[2], it is possible to show

[2] Y. Hatwalne, S. Ramaswamy, M. Rao, and R.A. Simha. Rheology of active-particle suspensions. Phys. Rev. Lett., 92:118101, 2004.

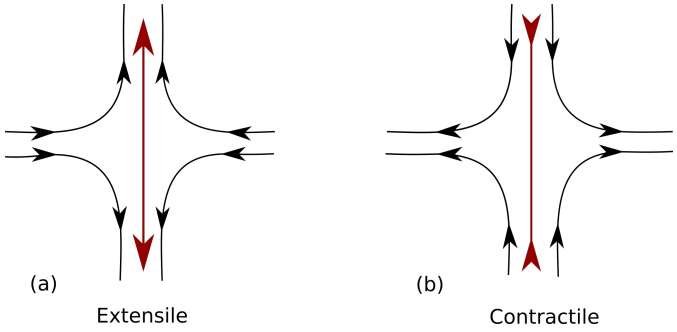

Figure 2: Cartoon of (a) extensile and (b) contractile flow (black lines), and force dipoles (red arrows).

that the stress exerted by the active agents can be expressed as

$$\underline{\underline{\sigma}}^{act} = -\zeta \left(\boldsymbol{P} \otimes \boldsymbol{P} - \frac{\boldsymbol{I}}{3} \boldsymbol{P}^2 \right),$$

where ζ is the active parameter or simply activity that rules the intensity of the stress exerted by the active agents. The sign of ζ allows to distinguish between extensile ($\zeta > 0$) and contractile ($\zeta < 0$) suspensions.

In the follwing I will present some studies on a polar active emulsion, whose equilibrium property is encoded in the following free-energy, a generalization of the Landau-Brazovskii theory, coupled to the De Gennes theory for liquid crystals [1,2]:

$$\begin{aligned} \mathcal{F}\left[\phi, \boldsymbol{P}\right] = \int \mathrm{d}\boldsymbol{r} \Bigg[& \frac{a}{4\phi_{cr}^2}\phi^2(\phi-\phi_0)^2 + \frac{k_\phi}{2}(\nabla\phi)^2 + \frac{c}{4}(\nabla^2\phi)^2 \\ & -\frac{\alpha}{2}\frac{(\phi-\phi_{cr})}{\phi_{cr}}\boldsymbol{P}^2 + \frac{\alpha}{4}\boldsymbol{P}^4 + \frac{k_P}{2}(\nabla\boldsymbol{P})^2 + \beta\boldsymbol{P}\cdot\nabla\phi \Bigg]. \end{aligned} \tag{6}$$

Here the first term is a double well potential for the concentration field allowing for the phase separation of the two fluids when $a > 0$, the gradient term propotional to $k_\phi < 0$ sets the surface tension that is negative in this case to favour the formation of interfaces, while the last term is required for thermodynamic stability. The polarization field $\boldsymbol{P}$ is confined in those regions where $\phi > \phi_{cr}$, while the gradient term for $\boldsymbol{P}$ defines the elastic properties of the polar liquid crystal. The last term anchors the polarization field to the interfaces (anchoring is tangential if $\beta < 0$ or hometropic if $\beta > 0$). The theory has a transition to a lamellar phase for $a < \frac{k_\phi^2}{4c} + \frac{\beta^2}{k_P}$, for symmetric compositions of the mixture [6]. In what follows I set the parameters of the free energy to ensure to be deeply in the lamellar phase. A typical configuration of the passive system during the relaxing dynamics is given in Fig 3 (left panel) [2]. When the composition of the mixture is sufficiently asymmetric, the lamellar pattern becomes unstable and gives way to an emulsion of droplet of the minority component in a matrix of the majority phase [1,3,4].

In all the studies that will be presented in the following the dynamical equations have been solved making use of a hybrid lattice Boltzmann algorithm, where the hydrodynamics is solved making use of a pure Lattice Boltzmann approach, while the dynamics of the order parameters is integrated through a finite difference algorithm. The basic features of the lattice Boltzmann method are summarized in the following paragraph.

The lattice Boltzmann Method The lattice Boltzmann approach to hydrodynamics is based on a phase-space discretized form of the Boltzmann equation for the distribution func-

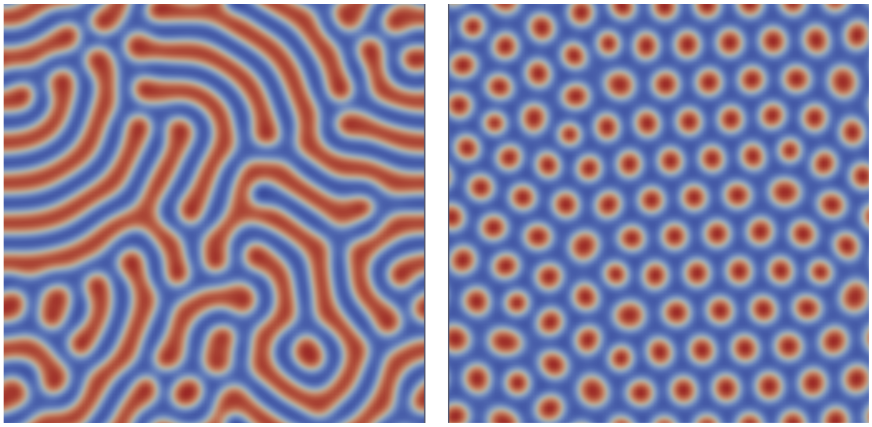

Figure 3: Configuration of a polar binary mixture during the relaxing dynamics for symmetric and asymmetric compositions, respectively shown in the left and right panels.

tion $f(\vec{r}, \vec{\xi}, t)$, describing the fraction of fluid mass at position $\vec{r}$ moving with velocity $\vec{\xi}$ at time t. Since discretization is performed both in real and velocity space, the algorithm is expressed in terms of a set of discretized distribution functions $\{f_i(\vec{r}_\alpha, t)\}$, defined on each lattice site $\vec{r}_\alpha$ and related to a discrete set of N lattice speeds $\{\vec{\xi}_i\}$, labelled with an index i that varies from 1 to N. In the case of the *collide and stream* version of the algorithm, the evolution equation for the distribution functions has the form

$$f_i(\vec{r} + \vec{\xi}_i \Delta t, t + \Delta t) - f_i(\vec{r}, t) = \mathcal{C}(\{f_i\}, t), \tag{7}$$

where $\mathcal{C}(\{f_i\}, t)$ is the collisional operator that drives the system towards equilibrium, represented by a set of equilibrium distribution functions. Assuming the BGK approximation with a single relaxation time, one writes

$$\mathcal{C}(\{f_i\}, t) = -\frac{1}{\tau}(f_i - f_i^{eq}), \tag{8}$$

where f_i^{eq} are the equilibrium distribution functions and τ is the relaxation time, connected to the viscosity of the fluid. The mass and momentum density are defined as

$$\rho(\vec{r}, t) = \sum_i f_i(\vec{r}, t), \tag{9}$$

$$\rho(\vec{r}, t)\vec{v}(\vec{r}, t) = \sum_i f_i(\vec{r}, t)\vec{\xi}_i, \tag{10}$$

where summations are performed over all discretized directions at each lattice point. By assuming both mass and momentum density to be conserved in each collision, it is found that conditions in Eq. (9), (10) must hold also for the equilibrium distribution functions:

$$\rho(\vec{r}, t) = \sum_i f_i^{eq}(\vec{r}, t), \tag{11}$$

$$\rho(\vec{r}, t)\vec{v}(\vec{r}, t) = \sum_i f_i^{eq}(\vec{r}, t)\vec{\xi}_i. \tag{12}$$

Moreover, it is necessary to introduce further constraints on the second moment of the equilibrium distribution functions to recover continuum equations:

$$\sum_i f_i^{eq} \xi_{i\alpha} \xi_{i\beta} = -\sigma_{\alpha\beta} + \rho v_\alpha v_\beta. \tag{13}$$

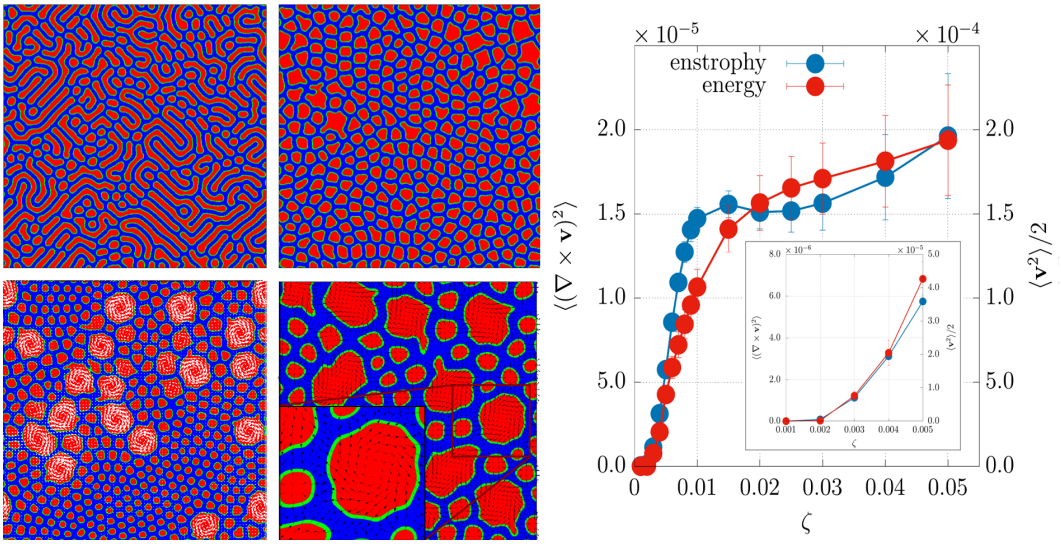

Figure 4: (Left) Late time contour plots of ϕ for $50:50$ extensile mixtures. (Top, left) $\zeta = 0.001$; (top, right) $\zeta = 0.002$; (bottom, left) $\zeta = 0.003$; (bottom right) $\zeta = 0.004$. Extensile activity leads to an emulsion of active droplets within a passive background. For moderate activity larger droplets rotate, as depicted by white velocity vectors in the bottom left panel. The zoom at $\zeta = 0.004$ illustrates typical polarisation patterns (black vectors in bottom the right panel) that have either an aster-like structure in small non-rotating droplets or a spiral shape in big rotating ones. (Right) Plot of the mean kinetic energy and of the mean enstrophy for several values of the extensile activity.

Further details of the numerical implementations can be found in [5]. In the following Sections I will be concerned with the analysis of the behavior of the system here presented in presence of activity. In particular I will report on the morphological transitions induced by extensile and contractile activity, while the final Sections will be respectively devoted to the rheological properties of extensile emulsions and the features characterizing the fully developed turbulent state.

3 Morphology of active emulsions

Experiments and numerical simulations performed on active matter suggest that three dynamical regimes develop in active gels at varying the activity parameter ζ: a quiescent regime where dissipative effects locally dissipate energy injected by activity and no flow is developed, an intermediate regime where elastic and active effects counterbalance and eventually give rise to spontanoeus flow and periodic behaviors, and finally a chaotic regime when activity overcomes reactive effects and push the system towards a turbulent-like state. The transition from the quiescent state first towards the spontaneous motion regime then to active turbulence strongly affects the morphology of active emulsions.

Extensile mixtures In the present Section I consider the case in which the active component is extensile ($\zeta > 0$) [2]. Upon increasing ζ the lamellar phase immediately gives way to an emulsion of active droplets within a passive background (Fig. 4) – the inverse of what happens in contractile mixtures. The active droplet emulsion is approximately monodisperse for $\zeta = 0.002$ (top right panel), and bidisperse for $\zeta = 0.003$ (bottom left panel). The transition between the lamellar

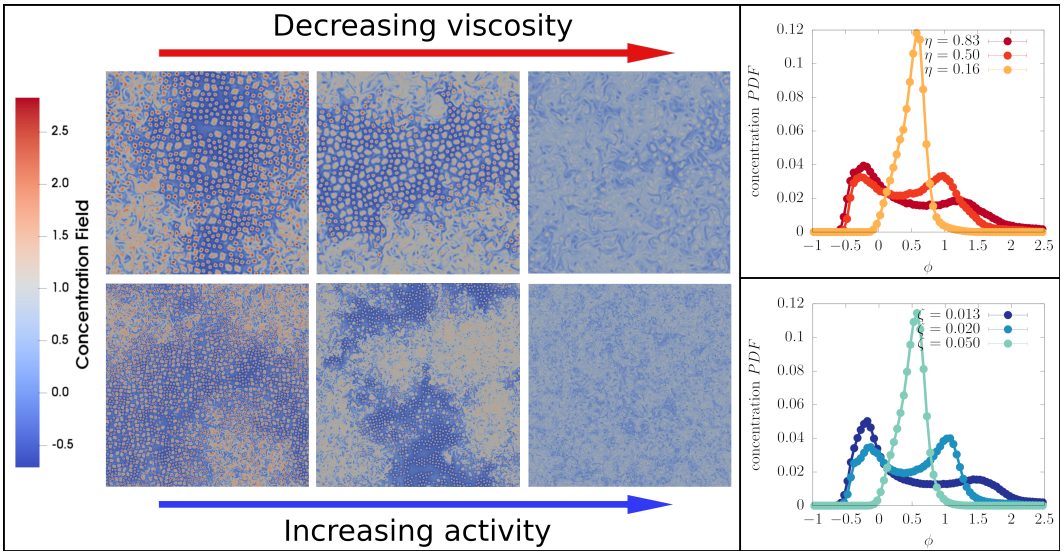

Figure 5: (Top-Bottom) Late time contour plots of ϕ for 25 : 75 extensile mixtures and its *pdf* at varying viscosity-activity.

and emulsion morphologies corresponds to the value of activity for which the mean enstrophy and kinetic energy depart from zero, $\zeta_{cr} \simeq 0.002$. The droplet size increases monotonically with the activity parameter – again the opposite behaviour of contractile mixtures. At very large ζ there is a crossover to macroscopic phase separation between active and passive components (corresponding to the plateau in the enstrophy and kinetic energy plots in Fig. 4), whereas for higher values of ζ the demixing process stops.

4 Active Turbulence in Extensile Emulsions

In this Section I will present some results concerning the setup of active turbulence in an asymmetric active emulsion where the active and passive phase are in a ratio of 25 : 75 [8]. In this case the equilibrium configuration of the system is not anymore showing lamellar patterns but an emulsion of droplets of the minority component in a majority background that arrange in an hexaticly orered fashion, eventually with some lattice defects in the whole pattern (see for instance the right panel of Fig. 3). As activity is switched on fluxes strengthen throughout the system and, analogously to what happen in the contractile symmetric case, they favor the elimination of topological lattice defects. Eventually, the system ends up in a defect free configuration at low-intermediate values of activity. Nevertheless, when ζ is increased over a certain threshold, droplets of active material may merge giving way to the onset of bending instabilities of the confined polar liquid crystal. This, firstly brings the droplet to rotate in a similar fashion as in the bottom contour plots of Fig. 4 but when activity is further increased the system undergoes a new morphological transition towards a total mixed phase, different from the one previously analyzed. This is due to the fact that strengthening the doping, induces more and more active stress across the droplets leading to interface breaking and droplet coalescence. The consecutive dispersion of active agents in the whole volume has the important effect to change the typical flow length-scales since small-scale deformation of the polarization pattern are wiped out.

Fig. 5 shows that the increase of the activity parameter is basically equivalent to an effective

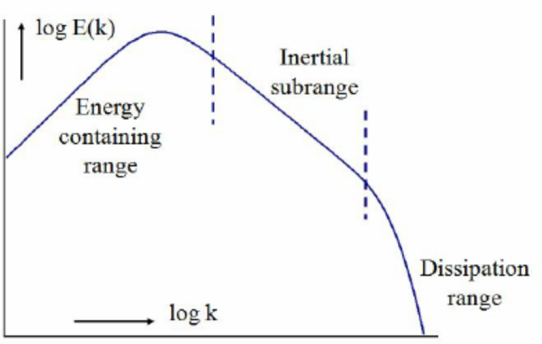

Figure 6: Typical energy spectrum of a turbulent flow in a newtonian fluid.

reduction of the viscosity of the mixture. This suggests an analogy between the mechanism driving newtonian fluids towards hydrodynamic turbulence and the chaotic dynamics of active gels.

Hydrodynamic turbulence is the last open problem in classical physics and no comprehensive theory has ever been formulated so far. The main problem concerning turbulence is the onset of hydrodynamic instabilities driven by the non-linear advection term $(\boldsymbol{v}\cdot\nabla\boldsymbol{v})$ in the Navier-Stokes equation. For a newtonian fluid there exists a single control parameter that is the Reynolds number

$$Re = \frac{l^* v^*}{\eta},$$

where l^* and v^* are respectively the typical length and speed of the flow, while η is the shear viscosity appearing in the viscous stress tensor. When the Reynolds number is low (hence when the velocity is very low or the flow length-scales are small so that dissipation phenomena overcome momentum advection) the fluid is in the laminar regime and flows in an ordered fashion; but when $Re \gtrsim 2700$ the transition to turbulence occurs, since energy is advected through different length-scales until it is dissipated at the micro-scales by viscous (molecular) phenomena.

To better understand the partition of energy between different length-scales it is custom in fluid-dynamics to study the statistical properties of the flow by looking at the energy spectrum, namely the spherical averaged structure factor of the flow field:

$$E(k) = \langle \boldsymbol{v}(\boldsymbol{k})^* \cdot \boldsymbol{v}(\boldsymbol{k}) \rangle,$$

where $\boldsymbol{v}(\boldsymbol{k})$ is the Fourier transform of the velocity field, and $\langle\cdot\rangle$ denotes spherical average. The typical shape of the energy spectrum is shown in Fig. 6. Three different regions can be found: at large length-scales (hence at low wave-numbers) the spectrum increases towards the peak where energy is accumulated and for this reason is usually addressed as *energy containing range*. This lenght-scale usually corresponds to the typical scale where energy is pumped into the system. In the *inertial range* energy is transferred by means of advective phenomena towards smaller scales, where viscosity will dissipate energy by means of friction mechanisms (the range of scales where viscosity becomes important is then addressed as *dissipation range*). According to Kolomogorov's theory, the flow must be self-similar in the inertial range where the only effective mechanism is the energy transfer due to the advective non linearity. By simple dimensional arguments, Kolmogorov proved that the energy spectrum in this range must satisfy the power low

$$E(k) \sim k^{-5/3},$$

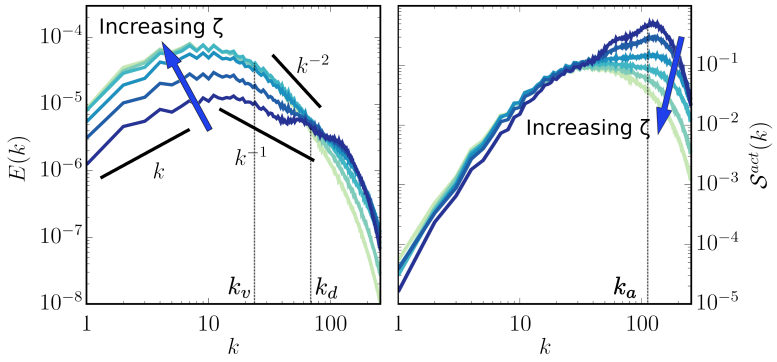

Figure 7: (Left) Left: log-log plot of time-averaged energy spectra varying activity ($\zeta = 0.013, 0.015, 0.02, 0.03, 0.04, 0.05$). Right: total amount of energy injected in the system by active agents. Vertical black dashed lines mark the wavenumber k_v , k_d and k_a respectively (see text) for the case at $\zeta = 0.05$.

a trand that is the universal fingerprint of fully developed hydrodynamic turbulence and it is found in any turbulent newtonian fluid.

In what follows I will present the results of my study on active turbulence that I performed by applying typical hydrodynamic methods the system previously presented to answer a question concerning the real nature of active turbulence. The main point concerning the chaotic dynamics in biological fluids is that their typical Reynolds number is much inferior than 1, so that the developement of a turbulent dynamics is a higlhly surprising phenomenon and the mechanisms that drive the system in the chaotic state still partially unknown.

In the active emulsion here considered the scaling properties of the energy spectrum $E(k)$ are not universal since they depend on the activity parameter ζ (see for instance left panel of Fig. 7). The right panel of the same figure shows the spectral properties of the active energy injection:

$$\mathcal{S}^{act}(k,t) = \langle \mathbf{v}^*(\mathbf{k},t) \cdot \mathbf{F}^{act}(\mathbf{k},t) \rangle \tag{14}$$

where $\mathbf{F}^{act}(k,t) = 2\pi i \mathbf{k} \cdot \tilde{\sigma}^{act}(\mathbf{k},t)/L$.

Energy pumping is considerably localized at high wavenumber ($k_a/L = l_a^{-1} \simeq 0.1$, where k_a stands for the first moment of $\mathcal{S}^{act}(k,t)$) when activity is low enough, due to small-scale deformations of the polarization field. By increasing ζ, as the system undergoes first coalescence ($\zeta = 0.02$), then mixing, interfaces broaden and progressively disappear, thus attenuating energy supply at high wavenumbers and leading to a situation where energy is injected on a wider range of scales, typical of the active-driven bending instabilities of the polar gel. Going back to the spectra, we can see that as long as the droplet phase survives, energy is accumulated on the typical length-scale of the droplet size ($l_d \simeq 15$) As confinement is lost ($\zeta \gtrsim 0.030$), energy is instead spread on much larger scales ($k_v/L = l_v^{-1} \simeq 0.025$, where k_v is the first moment of the energy spectrum $E(k)$). Even more interesting, is the observation that the energy injected in the system at low activity is substantially greater than the one delivered at higher active dopings.

This surprising behavior (and its connection to morphology) has been confirmed by keeping fixed the active parameter $\zeta = 0.015$ and varying the nominal viscosity of the suspension (not shown). Once again the total kinetic energy rises and develops on progressively bigger length-scales as viscous effects are lowered and mixing of the two components occurs, thus driving the active agents in an unconfined state.

I also performed a systematic analysis of the energy balance in Fourier space, by looking at the scale-by-scale contribution of all terms, either dissipative or reactive. To do this I considered

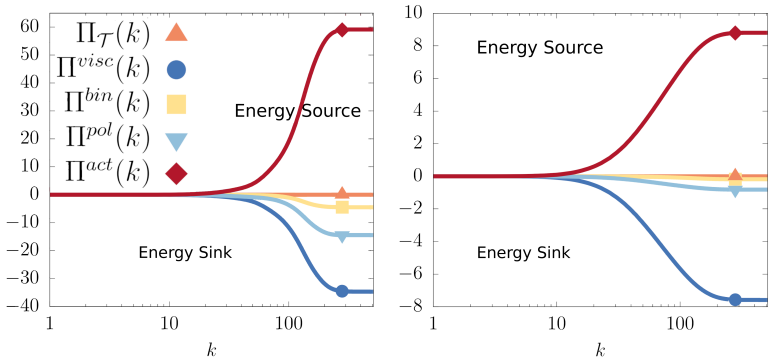

Figure 8: Time-averaged components of the total energy flux at $\zeta = 0.013$ (left panel) and $\zeta = 0.050$ (right panel). Notice the different y-range in the two graphs.

the Fourier-transformed version of the Navier-Stokes equation, spherically averaged on shells of equal momentum to obtain a balance equation for the kinetic energy:

$$\rho \partial_t E(k,t) + \mathcal{T}(k,t) = \sum_i \mathcal{S}^{(i)}(k,t). \tag{15}$$

Here $\mathcal{T}(k,t) = \langle \mathbf{v}^*(\mathbf{k},t) \cdot \mathbf{J}(\mathbf{k},t) \rangle$ represents the rate of energy transfer due to nonlinear hydrodynamic interactions (with $\mathbf{J}(\mathbf{k},t)$ standing for the Fourier transform of $\rho\mathbf{v} \cdot \nabla\mathbf{v} + \nabla p$). The terms on the right-hand side of Eq. (15) are energy source/sink contributions, where the terms $\mathcal{S}^{(i)}(k,t)$ are defined as in Eq. (14) and (i) denotes the different kinds of contributions (viscous, binary, polar or active). Finally I define each separate component of the energy flux as the total variation per unit time of the energy contained in a sphere of radius k:

$$\Pi^{(i)}(k,t) = \int_0^k \mathrm{d}k' \; \mathcal{S}^{(i)}(k',t),$$

with $\Pi_{\mathcal{T}}(k,t)$ defined analogously. Fig. 8 shows fluxes for $\zeta = 0.013, 0.050$, measured at steady state. In both cases, the only source contribution is the active one, Π^{act} while all the others are energy sinks. Before the transition to mixing ($\zeta = 0.013$ left panel) the binary and polar terms are also contributing (as sinks). After, the dynamics is characterized by an almost perfect matching among viscous and active terms (right panel). The advection term, $\Pi_{\mathcal{T}}$, is, for all practical effects, null, as expected for fluids flowing at negligible Reynolds numbers. The previous findings suggest some important conclusions. First, the scenario is in agreement with the absence of hydrodynamic turbulence. Here, multi-scale effects and chaotic evolution arise from the competition between sink terms and active injection leading to a non trivial scale-to-scale balance. The phenomenology is similar to the case of elastic turbulence, where the non-linear evolution for the velocity field is dominated by the non-Newtonian stress. Second, the efficiency of energy injection seems to be extremely increased as activity grows, thus suggesting a wide rheological phenomenology. Next Section will be focused on this issue.

5 Rheology of Extensile Emulsions

In order to study the rheology of the active emulsion I considered a symmetric extensile emulsion (whose morphological features have already been analyzed in Section 3) under an externally

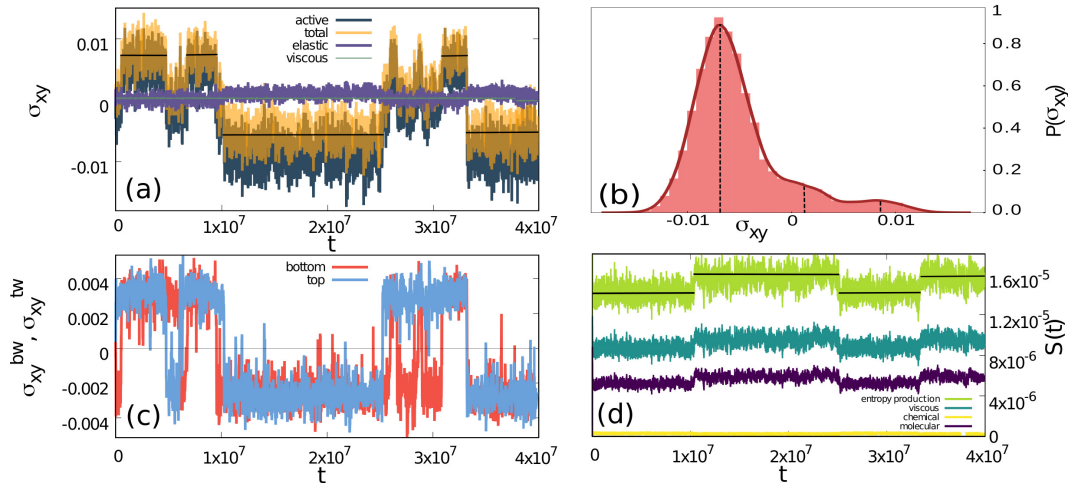

Figure 9: *Entropy production in multistable states.* (a) Time evolution of stress contributions at $Er_{act} = 1.14$,$Er = 0.00075$. The total stress is plotted in transparent yellow, while the active one is the dark blue curve underneath. Panel (b) shows the *pdf* of the total stress (data from 40 independent runs, fitted by 3 normal distributions peaked at $\sigma_{xy} = -0.0068, 0.0009, 0.0086$). (c) Total stress close to bottom and top walls, respectively computed as $\sigma_{xy}^{tw} = \int dx \int_{Ly-l}^{Ly} dy\ \sigma_{xy}$ and $\sigma_{xy}^{bw} = \int dx \int_{0}^{l} dy\ \sigma_{xy}$, where l is the width of the layer. Here $l = 15$. Nevertheless, as long as $l < Ly/2$, results remain unaltered. (d) Entropy production. Negative viscosity states, corresponding to **--** configurations of polarization at the boundaries, live longer than others. Entropy production $s(t)$ assumes greater values in correspondence of these regions.

imposed shear flow [6]. To do this I confined the system between two parallel moving walls with no-slip boundary conditions. The two walls move in opposite directions with velocity $\pm v_w$ so that the shear rate is given by $\dot{\gamma} = \frac{2v_w}{L}$, being L the channel width. Strong parallel anchoring was imposed for the polarization field at the wall site. In order to compare external and active forcing I consider the Ericksen number $Er = \eta_0 \dot{\gamma}/B$, and the active Ericksen number $Er_{act} = \zeta/B$, where B is the lamellar compression modulus, namely the energy cost for the variation of the lamellar width per unit length.

The most interesting behavior is found for large values of both shear rates and activity. Under this conditions the system exhibits an intermittent flow regime. This is to be related with the polarization configuration at the walls site ($\boldsymbol{P}$ can be parallel or antiparallel to the velocity on each wall, or can be parallel on a wall and antiparallel to the other and I will denote these three state with the notation $++$, $--$ and $+-$ respectively). During the evolution the system jumps between these three states. Such intermittent behavior is reflected in the evolution if the averaged stress as shown in Fig. 9. Elastic contributions are on average constant, while active stress fluctuates around positive, negative or vanishing values that also correspond to $++$, $--$ and $+-$ states respectively. These are found to be largely determined by the portion of the system closer to boundaries. Nevertheless, not all the states are equally probable: as shown by the *pdf* of the stress tensor in panel (b), thus suggesting the $--$ states to be more likely to occur than others. In order to better characterize the physics beyond this multistable dynamics I considered the different entropy production contributions are shown due to reactive, dissipative and source effects. We first notice that the contribution due to diffusion/chemical (yellow line) is almost null. In addition, the viscous dissipation (blue line) is always greater than the contribution due to the molecular field (violet line). This suggests that the hydrodynamics

of the system – driven by active injection and external forcing – is mainly countered by viscous dissipation phenomena. Moreover, the total entropy production oscillates around two different values and jumps during time evolution, with the highest value corresponding to the negative viscosity states. This behaviour is compatible with a maximum entropy production principle (MaxEPP).

Conference and Workshops

- APS - Division of Fluid Mechanics 2018; Atlanta (USA)
- XXIII National Conference on Statistical Physics and Complex Systems; Parma
- FisMat2019 - Catania

Publications

1 G. Negro, **L.N. Carenza**, P. Digregorio, G. Gonnella, and A. Lamura. Morphology and flow patterns in highly asymmetric active emulsions. Physica A, 503:464 – 475, 2018.

2 F. Bonelli, **L.N. Carenza**, G. Gonnella, D. Marenduzzo, E. Orlandini, and A. Tiribocchi. Lamellar ordering, droplet formation and phase inversion in exotic active emulsions. Scientific Reports, 9, 2019.

3 **L.N. Carenza**, G. Gonnella, A. Lamura, G. Negro. Dynamically asymmetric and bicontinuous morphologies in active emulsions, International Journal of Modern Physics C, 2019.

4 G. Negro, **L.N. Carenza**, P. Digregorio, G. Gonnella, A. Lamura. In silico characterization of asymmetric active polar emulsions, AIP Conference Proceedings 2071 (1), 020012, 2019.

5 **L.N. Carenza**, G. Gonnella, A. Lamura, G. Negro, A. Tiribocchi. Lattice Boltzmann methods and activefluids.Eur. Phys. J. E, 42(6):81, 2019.

6 G. Negro, **L.N. Carenza**, A. Lamura, A. Tiribocchi and G. Gonnella. Rheology of active polar emulsions: from linear to unidirectional and unviscid flow, and intermittent viscosity. Soft Matter, 2019.

7 **L.N. Carenza**, G. Gonnella, D. Marenduzzo, G. Negro. Rotation and propulsion in 3d active chiral droplets. PNAS (on press).

8 **L.N. Carenza**, G. Gonnella, L. Biferale. Multi-scale control of active emulsion dynamics. arXiv:1906.05968, 2019.

Teaching

- Peer Tutor 2018/2019